Available online at www.sciencedirect.com

ScienceDirect

journal homepage: www.elsevier.com/locate/he

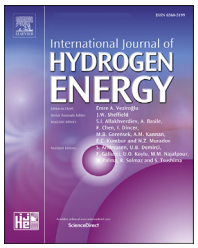

Modeling of the impact of cycling operating conditions on durability of polymer electrolyte fuel cells and its sensitivity analysis

Larisa V. Karpenko-Jereb [a], *Victor A. Kovtunenko* [b,c,*]

[a] *Scientific Consulting, Stattegg 8046, Austria*

[b] *Institute for Mathematics and Scientific Computing, Karl-Franzens University of Graz, NAWI Graz, Heinrichstr. 36, 8010, Graz, Austria*

[c] *Lavrentyev Institute of Hydrodynamics, Siberian Division of the Russian Academy of Sciences, 630090 Novosibirsk, Russia*

HIGHLIGHTS

- 1D Holby-Morgan model of platinum electrochemical degradation is applied.
- The catalyst degradation is computed at non-symmetric square voltage cycling.
- Simulations predict lifetime of Pt catalyst in low temperature PEM fuel cells.
- Variance-based analysis of operating conditions on Pt mass loss is carried out.
- Low temperature and ionomer ratio, high acidity and Pt size increase lifetime.

ARTICLE INFO

Article history:
Received 23 October 2022
Received in revised form
26 December 2022
Accepted 3 January 2023
Available online 25 January 2023

Keywords:
Polymer electrolyte fuel cell
Catalyst degradation
Platinum dissolution and oxidation
Electric potential cycling
Accelerated stress test
Variance-based sensitivity analysis
2010 MSC: 78A57, 80A30, 80A32, 35K57

ABSTRACT

In the paper, the impact on durability of polymer electrolyte membrane fuel cells is investigated when varying operating conditions applied in accelerated stress tests. By this, the electric potential cycling protocol in given by a non-symmetric square profile. The electrochemical degradation of a catalyst layer is caused by platinum ion dissolution and oxide coverage. These mechanisms are described by the one-dimensional Holby–Morgan model with a modified Butler–Volmer equation for the reaction rates. For efficient numerical solution of the underlying nonlinear reaction-diffusion system, a variable time-step implicit-explicit method is suggested. Computer simulations predict durability for the catalyst by using a linear extrapolation up to the full platinum surface blockage. A parameter sensitivity analysis is presented on different time scales and measures how the platinum mass loss is impacted by the variation of specific parameters.

* *Corresponding author.*
E-mail addresses: karpenkojereb@gmail.com (L.V. Karpenko-Jereb), victor.kovtunenko@uni-graz.at (V.A. Kovtunenko).

https://doi.org/10.1016/j.ijhydene.2023.01.029

Introduction

For high durability of polymer electrolyte membrane fuel cells (PEMFC), the actual tasks include studying degradation of valuable platinum catalysts [1–3], which are often used in commercially available vehicles and portable power sources. However, comparative analysis of experimental data is hardly possible, in particular, because industrial organizations explore quite different operating conditions. There are attempts to standardize protocols for PEMFC testing made by the European consortium on Fuel Cells and Hydrogen Joint Undertaking (FCH JU). In this respect, an intelligent way consists in mathematical modeling and numerical simulations for understanding of that electrochemical mechanisms causing the platinum surface degradation. We cite the studies [4–6] for diffusive models of Pt degradation in a PEM catalyst layer (CL). The relative modeling issues can be found, e.g., in Refs. [7–9] for Poisson–Nernst–Planck diffusion equations in multi-phase media with interface reactions, in Ref. [10] for the Butler equation, in Ref. [11] for mechanical fracture, and others.

Recently, Pahon et al. [12] published a comprehensive Review on Accelerated Stress Tests (AST) applied over the world to test chemical and mechanical durability of most important components of polymer electrolyte fuel cells: membranes, catalysator and catalyst layers, gas diffusion layers, bi-polar plates. The authors demonstrated the evolution in the AST elaboration and progress in developing mitigation strategies directed to prolong lifetime of materials.

Since Pt catalysators are high-priced materials in the fuel cells, degradation phenomena in catalysators and development of mitigation strategies are focus of numerous studies. Currently, the following degradation mechanisms have been known [2,12].

- Mechanical degradation of the catalyst layers usually caused by relative humidity (RH) cycling [13,14] or at stop/start-up operations [15]. The mechanical degradation reflects in surface cracking, delamination and particle detachment.
- Chemical degradation of ionomer leads to a decrease in proton conductivity of the catalyst layer, and, in this way, to reduction of the proton flux to the membrane.
- Corrosion of carbon support causes a drop of electron conductivity of the catalyst layer, and also leads to detachment of Pt particles. The intermediate product of the carbon corrosion, carbon monoxide CO, covers Pt/C catalyst, slowing the kinetics of Hydrogen Oxidation Reaction (HOR).
- Oxidation of Pt results in formation of PtO on the Pt particle, blocking the catalyst surface for Oxygen Reduction Reaction (ORR).
- Dissolution of Pt leads to formation of platinum (II) ions. One part of Pt-ions diffuses into the membrane, another part redeposits on neighbor particles. The mechanism of Pt ions redeposition is known as Ostwald ripening and leads to growth of the particle size.
- Migration and agglomeration of Pt particles: in order to reduce the higher surface energy caused by the smaller particle size, Pt nanoparticles usually migrate to agglomerate in larger particles.

All degradation mechanisms lead to a decrease in electrochemical active surface area (ECSA). Additionally, the ionomer degradation, detachment of the particles and diffusion of Pt^{2+} ions into the membrane result in mass loss of Pt in the catalyst layer.

Recently, Shokhen et al. [16] performed detailed analysis some mechanisms of Pt/C degradation in a single PEMFC, using identical location scanning electron microscopy (IL-SEM). The degradation was stimulated using ASTs with square wave voltage in a potential range of 0.6–1.0 V. The authors reported five different degradation processes of the platinum nanoparticles that were observed in the IL-SEM [16].

- Larger Pt particles tend to grow by absorbing dissolved material from smaller, less stable neighbor particles, via Oswald ripening.
- A minor percentage of the larger particles shrink to the point of not being visible by SEM.
- Particles grow until they merge with nearby neighbors.
- Some particles grow during the initial ASTs, after which they start to shrink during the later AST sessions.
- Particles close to each other tend to merge via crystallite migration and coalescence, whereas particles further away do not move toward each other. Particles that grow by crystallite migration tend to form elongated particles.

The development of mitigation strategies [17] for catalyst layers has been based on joint efforts on experimental investigations of material properties [18,19] and durability of fuel cell components [20–23], studies of degradation mechanisms [24], and also on modeling and simulation [13–15,25–28].

One of the promising tools to study of degradation mechanisms in the catalysts layers are simulation codes with physics-based models [4,5]. Usage of physics-based models allow researchers to analyze processes, which could been still undetectable by current instrumental techniques. Moreover, the models are enabling to get a lot of important information in quite short period of time and save valuable material and manpower resources. The modeling of degradation phenomena in catalyst layers of PEMFC started in 90s of last century and mainly described kinetics of Pt oxidation and dissolution. The current models enable to simulate almost all known mechanisms of degradation: C corrosion and particle agglomeration [29,30], diffusion of Pt ion in membrane [6,24,31], delamination [13–15,25,32]. The particle agglomeration significantly contributes to reduction of ECSA, therefore, a few attempts have been directed to create structural design of a nanocomposite catalyst layers with ultralow Pt loading [33–35] and to elaborate mitigation strategies to decelerate agglomeration process [36].

In our study we consider three mechanism of Pt/C catalyst degradation: Pt dissolution and oxidation, as well as Pt ion diffusion in the membrane. But, we neglect the growth of particle size. In thus way, we monitor mass loss of Pt, a decrease in the particle size, and estimate lifespan of Pt

catalyst limited by these three degradation processes. The present results will be important for developers of new types of catalysators based on arrays and possessing high durability to agglomeration and coalescence. As well the study could be important for developers, who direct their attempts to standardize protocols for PEMFC testing.

In future studies we are going to integrate in our model the effect of particle growth due the agglomeration and coalescence, in order to systematically study degradation effects caused by single mechanisms.

The considered platinum degradation model was suggested by Holby and Morgan [37] and developed further in Ref. [31]. By this, the PEM catalyst layer is assumed to be filled with Pt nano-particles, which are placed on a bound of carbon support with an ionomer. Recently, Shimanuki et al. [38] applied by cryogenic (cryo) SEM (scanning electron microscopy) and cryo-TEM (transmission electron microscopy) to study microstructure Pt/C catalyst binding with perfluorinated ionomer. As a result, the authors succeeded in observing the pore structure of the catalyst layer in the swollen state of the ionomer. The swollen ionomer surrounds and encloses he Pt/C aggregates and bridges over the pores in the catalyst layer. These experimental observations support the physical model of the catalyst structure. The Holby–Morgan model is based on two degradation mechanisms of the platinum ion (Pt^{2+}) dissolution and the platinum oxide (PtO) surface coverage according to the electrochemical reactions:

$$Pt_{(s)} \leftarrow\rightarrow Pt^{2+}_{(aq)} + 2e^{-}, \tag{1}$$

$$Pt_{(s)} + H_2O_{(aq)} \leftarrow\rightarrow PtO_{(s)} + 2H^{+}_{(aq)} + 2e^{-}. \tag{2}$$

The equations for (1) and (2) are described by modified Butler reaction rates providing for the Gibbs–Thomson effect in chemical potential. The Pt dissolution and oxidation takes into account diffusion of building Pt ions into the ionomer membrane directed across CL. This is worth noting that degradation would be impossible without the diffusion.

In the previous works [39,40] we employed the Holby–Morgan model for investigation of durability of PEMFC under cycling conditions with respect to different electric potential (called voltage) profiles used in the accelerated stress test (AST). Three industrial protocols were taken in the shape of a hat used by the U.S. Department of Energy (DOE), a square employed by Tennessee Tech University, and a triangle developed by Nissan. In the current work, we use the non-symmetric square voltage profile suggested recently within FCH JU programs (see Ref. [41]), as illustrated in Fig. 1 for three cycles.

The AST test in each cycle has $p = 40$ s long period and switches between the potential levels of $V_{min} = 0.6$ (V) during 10 s, and $V_{max} = 0.9$ (V) during 30 s. For numerical simulation of the degradation model we combine an implicit-explicit and variable time-step Runge–Kutta methods. For the square voltage profile, a step-size is refined locally at the electric potential lift-off from V_{min} to V_{max}. Indeed, lift-off of the electric potential increases contribution of the Pt ion diffusion over its transport, hence thermodynamic equilibrium is reached at a slower pace. The local refinement gives us a significant speed-up, thus advantage in the efficiency of numerical simulations compared to a uniform stepping used previously in Refs. [39,40].

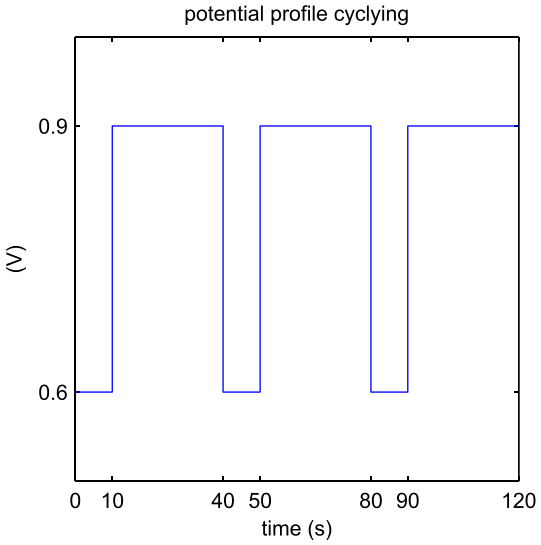

Fig. 1 – The profile of the square potential cycling considered in this study.

The CL model under consideration has in total about 30 input parameters representing PEMFC operating conditions. We aim to evaluate their impact on the degradation model output, which can be quantified by the rate of Pt mass loss during the electric potential cycling. Indeed, smaller platinum loss will lead to a higher lifetime of catalyst: when Pt mass becomes zero, then the fuel cell does not work anymore. From a point of view of statistics, global sensitivity analysis studies a simultaneous effect of multiple input parameters on the variance output. It can be described by Sobol sensitivity indexes usually estimated with Monte-Carlo methods (see e.g. Ref. [42]). A local sensitivity analysis focuses on how a single parameter perturbation impacts the output, known as one-variable-at-a-time (OAT) method. In the case of close to linear dependence, the Pearson correlation coefficient is reasonable for the sensitivity index (see Ref. [43]). We use the latter approach since a large number of input parameters.

A local sensitivity analysis is given for different 10, 100, 1000-cycle scales to measure how the platinum mass loss is correlated with the following parameters: temperature, pH value, ionomer volume fraction, Pt loading, particles diameter, and diffusion. In the sensitivity analysis, the upper and lower limits of the variable parameters are selected for research on the basis of their physical values, and the values taken from the literature. This variation of parameters results in about 3% loss of the initial Pt ion mass, that is right for local analysis. The coupling relationship between the operating conditions and parameters has to be analyzed further.

Model and methods

The physical model under our consideration is based on the following assumptions.

- a semi-infinite cathode catalyst layer (CL) in PEMFC is considered, which is posed between a gas diffusion layer (GDL) and a membrane;
- CL is filled with spherical Pt nano-particles placed on a carbon support and fully surrounded by perfluorinated sulfonated ionomer;
- all gaps and PEM are filled with the same ionomer;
- two degradation mechanisms account for Pt ion dissolution into surrounding, and formation of platinum oxides on the catalyst particle surface;
- platinum ions diffuse through the inonomer into PEM but not into GDL;
- all quantities of interest change along one dimension across CL and remain unchangeable in other directions.

Geometrically, we assume the space variable $x \in [0, L]$ across the CL of thickness L, such that the left end at $x = 0$ meets GDL, and the right end at $x = L$ confirms the interface with PEM. The parameters of Pt particles filling CL are gathered in Table 1.

The temperature T given on the Kelvin scale corresponds to 80 °C. The other physical parameters are taken from Ref. [39] and presented in Table 2 for platinum ion Pt^{2+} formation and diffusion, and in Table 3 for platinum oxide PtO formation. For further use we remind gas constant $R = 8.31445985$ J/(mol × K) and Faraday constant $F = 96485.3329$C/mol.

We remark that Tables 2 and 3 contain some fitting parameters taken from the literature and used for simulation.

Governing relations

For time $t \geq 0$, let the voltage $V(t)$ square profile in cycles be given according to Fig. 1 and express the electric potential difference versus a reference of 0 V. Across the catalyst thickness $x \in [0, L]$, we look for three unknown variables: platinum ion concentration $c(t, x) \geq 0$ (mol/cm^3), Pt particle diameter $d(t, x) \geq 0$ (cm), and platinum oxide coverage ratio $\theta(t, x) \in [0, 1]$ (dimensionless). The governing system of reaction-diffusion equations is formulated in Ref. [31] as follows:

$$\frac{\partial c}{\partial t} - \sqrt{\epsilon} D_{\mathrm{Pt}} \frac{\partial^2 c}{\partial x^2} = B_3 d^2 r_{\mathrm{dissol}}(c, d, \theta, V) \quad \text{for } t > 0,\ x \in (0, L), \tag{3}$$

where $B_3 = \pi N_{\mathrm{Pt}}/(2\epsilon)$ (1/cm^3) is denoted for short, and

$$\frac{\partial d}{\partial t} = -\Omega\, r_{\mathrm{dissol}}(c, d, \theta, V) \quad \text{for } t > 0,\ x \in (0, L), \tag{4}$$

$$\frac{\partial \theta}{\partial t} + \frac{2\theta}{d}\frac{\partial d}{\partial t} = \frac{1}{\Gamma} r_{\mathrm{oxide}}(\theta, V) \quad \text{for } t > 0,\ x \in (0, L). \tag{5}$$

The partial differential equations are endowed with the initial condition:

$$c = 0, \quad d = d_{\mathrm{Pt}}, \quad \theta = 0 \quad \text{as } t = 0,\ x \in [0, L], \tag{6}$$

and the mixed Neumann–Dirichlet boundary conditions:

$$\frac{\partial c}{\partial x} = 0 \quad \text{as } t > 0,\ x = 0, \quad c = 0 \quad \text{as } t > 0,\ x = L \tag{7}$$

implying no-flux condition at the GDL-CL interface, and zero concentration of dissolved ions at the CL-PEM interface.

Following [37] the reaction rates in (3)–(5) are based on a modified Butler equation, which describes in units of mol/(cm^2 × s) the Pt ion dissolution (1) by

$$\begin{aligned} r_{\mathrm{dissol}}(c, d, \theta, V) = {} & B_1(d, \theta)\exp\{(1 - \beta_1)B_4(d, \theta)V\} \\ & - cB_2(d, \theta)\exp\{-\beta_1 B_4(d, \theta)V\}, \end{aligned} \tag{8}$$

and the Pt oxide coverage (2) by

$$\begin{aligned} r_{\mathrm{oxide}}(\theta, V) = {} & \Gamma\exp\left\{-\frac{1}{RT}(H_{2,\mathrm{fit}} + \lambda\theta)\right\}\left(\nu_1^{\star}\left(1 - \frac{\theta}{2}\right)\exp\left\{-\frac{n_2 F(1 - \beta_2)}{RT}\left(U_{\mathrm{fit}} + \frac{\omega\theta}{n_2 F}\right)\right.\right. \\ & \left.\left. + (1 - \beta_2)\frac{n_2 F}{RT}V\right\} - \nu_2^{\star} 10^{-2pH}\exp\left\{\frac{n_2 F\beta_2}{RT}\left(U_{\mathrm{fit}} + \frac{\omega\theta}{n_2 F}\right) - \beta_2\frac{n_2 F}{RT}V\right\}\right). \end{aligned} \tag{9}$$

The equations (8) and (9) employ the auxiliary quantity B_1 given in mol/(cm^2 × s):

$$B_1(d, \theta) = \nu_1\Gamma(1 - \theta)\exp\left\{\frac{1}{RT}\left(-H_{1,\mathrm{fit}} - nF(1 - \beta_1)\left(U_{\mathrm{eq}} - \frac{4\Omega\gamma_0(\theta)}{nFd}\right)\right)\right\}, \tag{10}$$

the quantity B_2 (cm/s):

Table 1 – Parameters for cathode catalyst layer.

Symbol	Value	Units	Description
L	1×10^{-3}	cm	CL thickness
d_{Pt}	3×10^{-7}	cm	Pt particle diameter
V_{Pt}	1.5×10^{-20}	cm^3	Pt particle volume
ρ_{Pt}	21.45	g/cm^3	Pt particles density
p_{Pt}	4×10^{-4}	g/cm^2	Pt particles loading
ϵ_{Pt}	0.02		Pt volume fraction across CL
N_{Pt}	1.32×10^{18}	1/cm^3	Pt number concentration in CL
ϵ	0.2		volume fraction of ionomer increment in cathode
T	353.15	K	temperature

Table 2 – Parameters for Pt ion formation and diffusion.

Symbol	Value	Units	Description
ν_1	1×10^4	Hz	dissolution attempt frequency
ν_2	8×10^5	Hz	backward dissolution rate factor
β_1	0.5		Butler transfer coefficient for Pt dissolution
N	2		electrons transferred during Pt dissolution
U_{eq}	1.118	V	Pt dissolution bulk equilibrium voltage
Ω	9.09	cm^3/mol	molar volume of Pt
Γ	2.4×10^{-4}	J/cm^2	Pt [1 1 1] surface tension
c_{ref}	1	mol/cm^3	reference Pt ion concentration
$H_{1,fit}$	4×10^4	J/mol	fit Pt dissolution activation enthalpy
D_{Pt}	1×10^{-6}	cm^2/s	diffusion coefficient of Pt ion in the membrane

Table 3 – Parameters for Pt oxide formation.

Symbol	Value	Units	Description
pH	0		potential of hydrogen ions (protons)
$\nu_1^\star$	1×10^4	Hz	forward Pt oxide formation rate constant
$\nu_2^\star$	2×10^{-2}	Hz	backward Pt oxide formation rate constant
Γ	2.2×10^{-9}	mol/cm^2	Pt surface site density
β_2	0.5		Butler transfer coefficient for PtO formation
n_2	2		electrons transferred during Pt oxide formation
U_{fit}	0.8	V	Pt oxide formation bulk equilibrium voltage
Λ	2×10^4	J/mol	Pt oxide dependent kinetic barrier constant
Ω	5×10^4	J/mol	Pt oxide-oxide interaction energy
$H_{2,fit}$	1.2×10^4	J/mol	fit partial molar oxide formation activation enthalpy

$$B_2(d,\theta) = \frac{\nu_2 \Gamma(1-\theta)}{c_{ref}} \exp\left\{\frac{1}{RT}\left(-H_{1,fit} + nF\beta_1\left(U_{eq} - \frac{4\Omega\gamma_0(\theta)}{nFd}\right)\right)\right\}, \tag{11}$$

and the quantity B_4 (C/J):

$$B_4(d,\theta) = \frac{F}{RT}\left(n - \frac{4\Omega\Gamma n_2\theta}{d}\right), \tag{12}$$

where the expression of γ_0 in J/cm^2 is given by

$$\gamma_0(\theta) = \gamma + \Gamma RT\left(\theta \ln\left(\frac{\nu_2^\star}{\nu_1^\star}10^{-2pH}\right) + \theta\frac{2n_2FU_{fit} + \omega\theta}{2RT} + \theta\ln\left(\frac{\theta}{2}\right) + (2-\theta)\ln\left(1-\frac{\theta}{2}\right)\right). \tag{13}$$

All parameters employed in system (3)–(13) are collected in Tables 1–3.

Numerical methods

From a mathematical point of view, the numerical problem consists in solving the diffusion system (3)–(7) with nonlinear reactions of exponential type given by (8)–(13). For the physical consistency, Pt ion concentration and particle diameter cannot be negative, and Pt oxide coverage ratio should lie between 0 and 1. To preserve these non-negative thresholds during evolution, the time step had needed to be taken sufficiently small, otherwise the solution became negative and destroyed. To speed up the computation, we suggest local refinement at that times when the electric potential starts its lift-off, and coarse time steps otherwise. The combination of a 4th order Runge–Kutta (RK4) and a second order implicit-explicit scheme (IMEX2) described in Ref. [39] are applied for discretization of the diffusion system on the non-uniform time mesh. In the numerical tests we set the coarse time step to $\tau_{coarse} = 10^{-2}$ (s), and the uniform CL thickness spacing $h = L/10$ (cm). Whereas the fine time $\tau_{fine} = 10^{-4}$ (s) was sufficient inside $(-\tau_{coarse}, \tau_{coarse})$-neighborhood of the electric potential V(t) lift-off from 0.6 to 0.9 (V) at the time $t_{liftoff} = 10$ s during each period of $p = 40$ s (see Fig. 1).

During 3 cycles of the square voltage V(t) in Fig. 1, the corresponding solution triple (c, d, θ) is depicted versus time $t \in [0, 120]$ (s) and CL thickness $x \in [0, L]$ (cm) in Fig. 2 in plots (a), (b), and (c). In the plot (a) we observe that the Pt ions distribution $c(t, x)$ across the catalyst is varied periodically from 0 to around 3.2×10^{-7} (mol/cm^3). By this, the concentration is high at the left end meeting the interface with GDL, and low at the right end when approaching PEM. The plot (b) shows a decrease of Pt particle diameter $d(t, x)$ in time. The diameter values of Pt particle at the end of each cycle at the point $x = L$ are shown on z-axis. The diameter decreases faster right at the catalyst layer than at the left. In the plot (c) of Fig. 2, the oxide coverage $\theta(t, x)$ of the Pt surface is changed periodically from 0 to approximately 90%. In every cycle, the platinum oxide is formed at the high voltage V_{max}, and the reverse reaction reduces PtO to platinum at the low voltage V_{min}.

Results and discussion

On the basis of numerical simulations described in Section 2, we investigate the degradation of platinum by the cycling operating conditions.

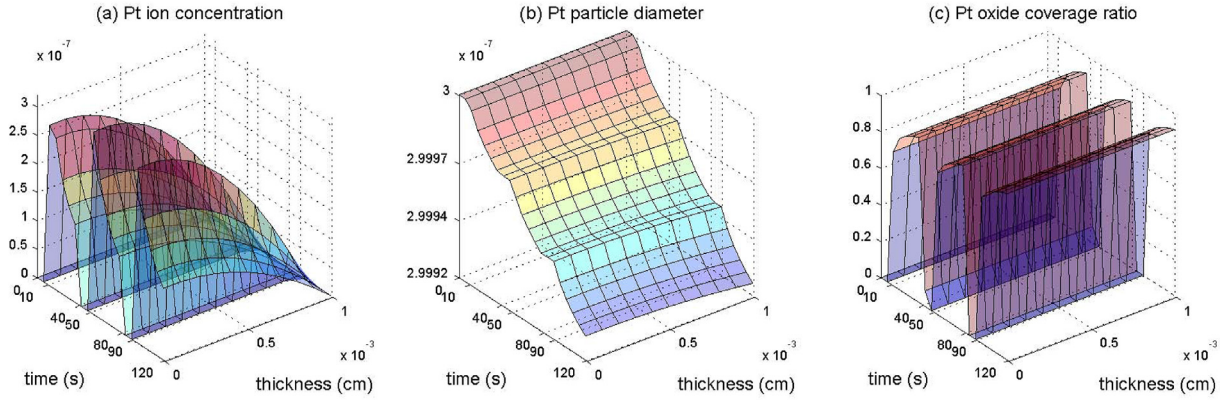

Fig. 2 – Pt^{2+} concentration c (a), Pt particle diameter d (b), PtO coverage ratio θ (c).

Pt mass loss

The electrochemical degradation of PEM can be measured by the relative Pt mass ratio $m_{Pt} \in [0, 1]$ defined for $t \geq 0$, $x \in [0, L]$ as

$$m_{Pt}(t, x) = \frac{4}{3}\pi\left(\frac{d(t, x)}{2}\right)^3 \Big/ V_{Pt} = \left(\frac{d(t, x)}{d_{Pt}}\right)^3, \tag{14}$$

which is found according to the Pt diameter $d(t, x)$ in (4), and scaled by the constant d_{Pt} due to the initial condition in (6) at $t = 0$. In Fig. 3 (a) we plot $m_{Pt}(t, x)$ from (14) along the catalyst thickness $x \in [0, L]$ during 10 cycles. In the plot we observe the decay in time of m_{Pt} starting at 1, which implies loss of platinum ions. The decay is weaker at the left end $x = 0$, and stronger at the right end $x = L$. The values of Pt mass ration at the end of even cycles at $x = L$ are shown on z-axis.

When averaged over the catalyst thickness, this quantity is expressed by

$$\bar{m}_{Pt}(t) = \underset{x\in[0,L]}{\text{mean}}(m_{Pt}(t, x)). \tag{15}$$

In Fig. 3 (b) and (c) we plot the averaged platinum mass ratio computed by formula (15) versus the number of cycles. The plots are given in two different time-scales. The curve for 10 cycles during 6 min. 40 sec. is depicted in the plot (b) and obeys a visible waving behavior in the fine scale. Whereas in the plot (c) the curve is continued for 1000 cycles during 11 h 6 min. 4 sec. and visually close to the straight line in the coarse scale. Based on the linear behavior, in the following we present the simulations carried on 100 cycles during 1 h 6 min. 4 sec.

A decrease in time of the Pt mass ratio during the voltage cycling effects the catalyst durability: smaller loss rate ensures larger durability, larger rate leads to drop. We study how important is the impact of operating conditions on the degradation behavior. For this task, we refer to the values of parameters fixed in Tables 1–3 and vary them in a suitable range using the OAT principle: one variable at a time. The result of $\bar{m}_{Pt}$ when varying the temperature $T \in \{60, 70, 80, 90\}$° C and acidity $pH \in \{0, 0.5, 1, 1.5\}$ is depicted in the left and right plots of Fig. 4.

The rise in the temperature from 60 °C to 90 °C results in 3% loss of the initial value $\bar{m}_{Pt}(0) = 1$ after 100 voltage cycles. Operating PEMFCs at relatively high temperatures has some advantages that include greater tolerance to CO, providing easier management of water and improved efficiency. Carbon monoxide is built on the carbon support surface due to incomplete oxidation of carbon. Higher temperature accelerates CO oxidation to CO_2. Water management is easier at higher temperature, because most part of water is found in vapour state and does not build liquid water droplets, which could lead to flooding effect in the gas diffusion layer.

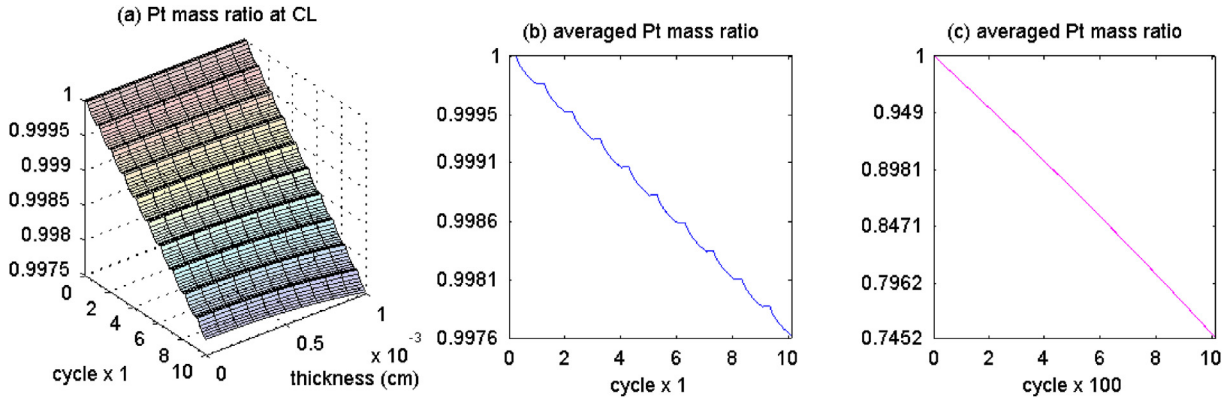

Fig. 3 – m_{Pt} during 10 cycles (a), $\bar{m}_{Pt}$ during 10 cycles (b), $\bar{m}_{Pt}$ during 1000 cycles (c).

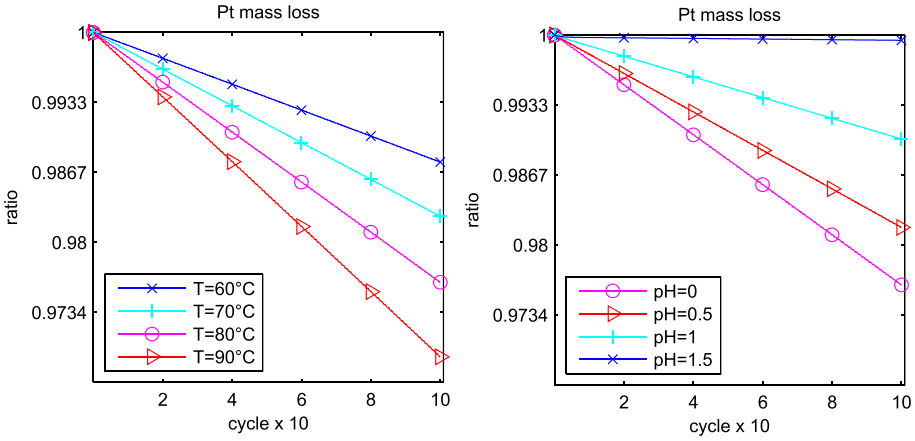

Fig. 4 – Pt loss depending on temperature (left) and acidity (right).

However, the increase in the operating temperature leads to acceleration of the Pt dissolution and to reduction of the catalyst lifetime as seen in Fig. 4. The tendency in the changes in the Pt mass loss as well as the lifetime duration at varying temperature is also demonstrated in Table 5. The rise in the temperature from 60 °C to 90 °C shortens the lifetime of Pt/C catalysator around in two and half time. In Ref. [44], Bi and Fuller investigated temperature effects on cathode Pt/C catalyst degradation using square-wave potential cycling between 0.87 V and 1.2 V. They observed rapid Pt/C degradation at higher temperatures. The Pt degradation results in lower performance, loss of Pt catalyst electrochemically active surface area, and deposition of Pt in the membrane.

The increase in acidity from pH = 0 to pH = 1.5 positively affects the Pt catalyst durability and prolongs its lifetime. The acidity is correlated with concentration of protons in the catalyst, which depends on the dissociation degree of the functional groups in the ionomer. The pH scale is logarithmic and inversely indicates the concentration of hydrogen ions in the solution

$$pH = -\log(a_{H^+}).$$

The acidity at the catalyst/ionomer interfaces depends on the dissociation degree of functional group of the ionomer, in the studied case it is Nafion. Nafion is a super-acid ionomer, the dissociation of its functional group is a function of water concentration in the membrane [45], and this water concentration increases with rising relative humidity (RH). Therefore, in the paper we speak about the relationship between pH and humidity. Since Nafion is very strong acid ionomer, it acidity pH usually lies between 0 and 1.5 [46]. The lower pH corresponds to a higher dissociation degree and a higher proton concentration. The dissociation degree increases with rising relative humidity. It means, higher relative humidity results in a lower acidity. In Ref. [44] Bi and Fuller investigated the loss rate of Pt mass at 60 °C at two different relative humidity: 50 and 100%. The investigation showed that at the higher RH the Pt dissolution is higher. These experimental results confirm the present simulation at different acidity: with growing acidity (a higher acidity, pH, is corresponding to a lower RH) the Pt mass loss decreases, that results in longer lifetime of Pt catalyst in the PEMFC. A significant increase of the cathodic dissolution with drop in pH was mentioned in Ref. [47].

In Fig. 5 we depict the variation of ionomer volume fraction $\epsilon \in \{0.1, 0.2, 0.3, 0.4\}$ and Pt loading $p_{Pt} \in \{1, 2, 3, 4\} \times 10^{-4}$ (g/cm^2) in the left and right plots, respectively.

In [48] authors reported acceleration of reversible degradation at cathodic Pt loadings $0.2 \le p_{Pt} \le 0.4$ (mg/cm^2). As seen from the figure, increasing the ratio of the ionomer in the catalyst layer, the Pt mass loss slightly rises. This effect is attributed with Pt dissolution process: the catalyst layer with a higher content of the ionomer provides more space for diffusion of Pt-ions occurring during the Pt dissolution reaction. The Pt loading practically does not affect the rate of the Pt mass loss.

Table 4 – Lifetime prognosis when varying operating conditions: temperature, acidity, ionomer volume fraction, Pt loading, particle diameter, diffusion coefficient.

Parameters	Pt loss rate $\times 10^{-6}$ (1/cycle)	Cycles (#)	Time (h)
$T = 80$ °C, pH = 0, $\epsilon = 0.2$, $p_{Pt} = 4 \times 10^{-4}$, $d_{Pt} = 3 \times 10^{-7}$, $D_{Pt} = 1$	237.89	4203	46.7
$T = 60$ °C	123.42	8102	90.0
$T = 70$ °C	175.08	5711	63.5
$T = 90$ °C	308.81	3238	36.0
pH = 1.5	4.99	200,547	2228.0
pH = 1	98.95	10,105	112.0
pH = 0.5	183.15	5460	60.7
$\epsilon = 0.1$	223.66	4471	49.7
$\epsilon = 0.3$	242.14	4130	45.9
$\epsilon = 0.4$	244.17	4095	45.5
$p_{Pt} = 3 \times 10^{-4}$ (g/cm^2)	239.41	4176	46.4
$p_{Pt} = 2 \times 10^{-4}$ (g/cm^2)	240.89	4151	46.0
$p_{Pt} = 1 \times 10^{-4}$ (g/cm^2)	242.56	4122	45.8
$d_{Pt} = 4 \times 10^{-7}$ (cm)	73.59	13,588	151.0
$d_{Pt} = 3.5 \times 10^{-7}$ (cm)	123.34	8107	90.0
$d_{Pt} = 2.9 \times 10^{-7}$ (cm)	277.74	3600	40.0
$D_{Pt} = 3.4 \times 10^{-6}$ (cm^2/s)	247.76	4036	44.8
$D_{Pt} = 6.7 \times 10^{-6}$ (cm^2/s)	249.84	4002	44.5
$D_{Pt} = 10 \times 10^{-6}$ (cm^2/s)	250.55	3991	44.3

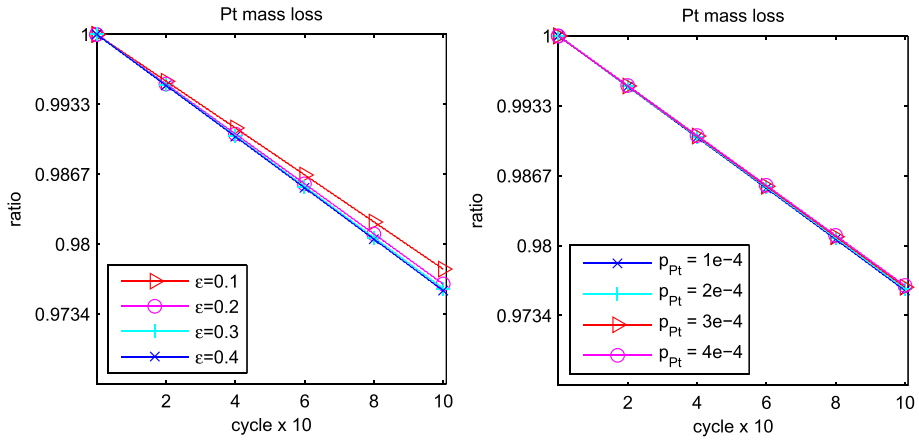

Fig. 5 – Pt loss depending on ionomer volume fraction (left) and Pt loading (right).

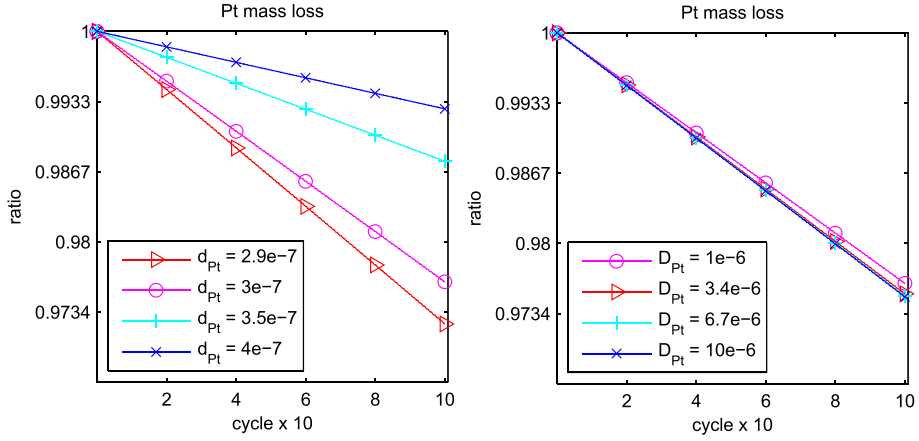

Fig. 6 – Pt loss depending on Pt particle diameter (left) and diffusion coefficient (right).

In the following Fig. 6 we depict the variation of Pt particle diameter $d_{Pt} \in \{2.9, 3, 3.5, 4\} \times 10^{-7}$ (cm) and diffusion coefficient $D_{Pt} \in \{1, 3.4, 6.7, 10\} \times 10^{-6}$ (cm^2/s).

The smaller Pt particle diameter 2.5 nm will lead to $\bar{m}_{Pt} = 0.94$ after 100 cycles, which is far below the range 0.9667 … 1 for the Pt mass loss plotted in the figures, hence the value 2.9 nm is set. As seen from the figure, with rising size of Pt particles the Pt mass loss decreases. It is connected with Gibbs–Thomson energy (GT) reflecting a change in the chemical potential of a particle as a function of diameter: GT energy grows with decreasing particle diameter [49]. Thus, the particles with a lower diameter dissolve easier than the particles with a bigger one. The model applied in this study takes into account the GT energy, and this consideration reflects in the simulation results: with growing Pt particle diameter the Pt mass loss decreases. Our simulation results agree with experimental data summarized by Cherevko et al. in Ref. [50]. The authors analyzed lifetime of Pt/C catalyst investigated at steady state and also at cycling voltage conditions published in Refs. [51–53]. The analysis showed, that both at steady state voltage and at cycling voltage the Pt dissolution rate is higher for Pt particles with a lower diameter. For example, the increase in Pt particle diameter from 2.2 nm to 5.0 nm rose the lifetime of Pt catalyst studied at triangle-cycling voltage 0.6–1.0 V in more than four times. In our simulation, studying the effect of the square cycle 0.6–0.9 V, the increase in the diameter from 3.0 nm to 4.0 nm raises the Pt durability more than in three times (see Table 4). Thus, these experimental observations are well verifying the simulation results. The studied values of the diffusion coefficient of the Pt ions practically does not affect the lifetime of the catalyst, as seen from Fig. 6 on the right.

Moreover, a linear decay of $\bar{m}_{Pt}$ allows us to predict a lifetime for the catalyst as follows. From the data depicted in Figs. 4–6, we calculate the rate of the averaged Pt mass loss

Table 5 – Variances and correlation coefficients for input and output parameters.

Parameter	Var(X)	Var($\bar{m}'_{Pt}$)	ρ_X
$X = p_{Pt}$	1.3×10^{-8}	3.00×10^{-12}	−0.999
$X = pH$	0.31	7.76×10^{-9}	−0.993
$X = d_{Pt}$	3.13×10^{-15}	3.87×10^{-8}	−0.976
$X = D_{Pt}$	1.15×10^{-11}	2.58×10^{-11}	0.844
$X = \epsilon$	0.01	6.41×10^{-11}	0.918
$X = T$	125	4.81×10^{-9}	0.997

(which is just the slope $\bar{m}'_{Pt}$ of the straight lines) and linearly extrapolate it with respect to a number of cycles up to $\bar{m}_{Pt} = 0$. At this time, no Pt particles remain on the carbon surface, and the catalyst layer does not work anymore. We present the lifetime prognosis in Table 4 in descending order with respect to the predicted number (#) of live cycles, respectively, hours of work. For comparison between the varied parameters, the reference parameters are given in the first row.

To compare the relative impact of operating conditions we apply parameter sensitivity analysis. Namely, we set the Pt mass loss rate $\bar{m}'_{Pt}$ found in simulations as the measured output from variation of input parameters X, and use the Pearson correlation coefficient

$$\rho_X = \frac{\mathrm{cov}\left(X, \bar{m}'_{Pt}\right)}{\sqrt{\mathrm{Var}(X)\mathrm{Var}\left(\bar{m}'_{Pt}\right)}} \in [-1, 1]. \tag{16}$$

By this, the magnitude of $|\rho_X|$ describes how sensitive is the model output $\bar{m}'_{Pt}$ to variation of the specific parameter X. Whereas the positive sign $\rho_X > 0$ indicates, that increase of X would increase the Pt mass loss, thus reduce a lifetime. Respectively, a negative sign $\rho_X < 0$ implies decrease of the platinum loss and raise of lifetime. For the selected six parameters $X \in \{T, \mathrm{pH}, \epsilon, p_{Pt}, d_{Pt}, D_{Pt}\}$ from Table 4, the corresponding correlation coefficients computed according to (16) are collected in ascending order in Table 5.

Conclusion

This paper is devoted to study the mass loss of Pt in the catalyst and catalyst lifetime in low temperature fuel cells at non-symmetric square cycling voltage 0.6–0.9 V. The mass loss of Pt and the catalyst lifetime are investigated at varying parameters: operating conditions as temperature and acidity; structural parameters as ionomer ratio, Pt particle size, Pt loading; and the transport characteristics of Pt ions — Pt diffusion coefficient. The study is performed using the one-dimensional Holby–Morgan model with a modified Butler–Volmer equation considering the effect of Gibbs–Thomson energy on the reaction rates. This model has been already applied in our previous papers to investigate Pt catalyst lifetime for different protocols of Accelerated Stress Tests [39] and at varying profile of voltage cycling [40].

We use the same 1D model, which has been used in previous research, in order to obtain a systematical analysis on impact of different factors on the CL degradation. This analysis should be a basis for understanding of the model and also for its further development. In order to analyze the degradation state in space, we have to couple this 1D model with a 3D performance model, often applied in CFD simulation. In this case, all operating conditions required for the calculation in the Pt degradation model should be considered locally. The local operating conditions strongly depend on the design of fuel cells. We can assume that at inlet of O_2 or air, the degradation rate of Pt will be higher due to increased temperature and higher O_2 concentration. According to the model, at points with higher water concentration and higher temperature, the Pt degradation will be accelerated.

The present simulation results show that rising temperature speeds up Pt mass loss, the increase in acidity slows down the Pt dissolution, the higher ionomer ratio slightly accelerates the Pt degradation. The Pt mass loss is strongly depending on the Pt particle size. The smaller particles are exposed to higher dissolution rate due to Gibbs–Thomson energy. In the investigated ranges of Pt loading and diffusion coefficient of Pt ions we do not detect any pronounced effects on the Pt mass loss and lifetime.

Our theoretical results are consistent with experimental results documented in the literature on durability of fuel cells [44,47–50].

Declaration of competing interest

The authors declare that they have no known competing financial interests or personal relationships that could have appeared to influence the work reported in this paper.

REFERENCES

[1] Eikerling M, Kulikovsky A. Polymer electrolyte fuel cells. Amsterdam: Elsevier; 2017.

[2] Hacker V, Mitsushima S. Fuel cells and hydrogen. Amsterdam: Elsevier; 2018.

[3] Kulikovsky A, Berg T. Positioning of a reference electrode in a pem fuel cell. J Electrochem Soc 2015;162(8):F843–8. https://doi.org/10.1149/2.0231508jes.

[4] Karpenko-Jereb L, Sternig C, Fink C, Tatschl R. Membrane degradation model for 3D CFD analysis of fuel cell performance as a function of time. Int J Hydrogen Energy 2016;41(31):13644–56. https://doi.org/10.1016/j.ijhydene.2016.05.229.

[5] Karpenko-Jereb L, Araki T. Modeling of polymer electrolyte fuel cells. In: Hacker V, Mitsushima S, editors. Fuel cells and hydrogen. Amsterdam: Elsevier; 2018. p. 41–62. https://doi.org/10.1016/B978-0-12-811459-9.00003-7. Ch. 3.

[6] Pandy A, Yang Z, Gummalla M, Atrazhev V, Kuzminyh N, Sultanov V, Burlatsky S. A carbon corrosion model to evaluate the effect of steady state and transient operation of a polymer electrolyte membrane fuel cell. J Electrochem Soc 2013;160(9):F972. https://doi.org/10.1149/2.036309jes. –F979.

[7] Fellner K, Kovtunenko V. A discontinuous Poisson–Boltzmann equation with interfacial transfer: homogenisation and residual error estimate. Appl Anal 2016;95(12):2661–82. https://doi.org/10.1080/00036811.2015.1105962.

[8] González-Granada J, Kovtunenko V. Entropy method for generalized Poisson–Nernst–Planck equations. Anal Math Phys 2018;8(4):603–19. https://doi.org/10.1007/s13324-018-0257-1.

[9] Kovtunenko V, Zubkova A. Mathematical modeling of a discontinuous solution of the generalized Poisson–Nernst–Planck problem in a two-phase medium. Kinet Relat Models 2018;11(1):119–35. https://doi.org/10.3934/krm.2018007.

[10] Dreyer W, Guhlke C, Müller R. A new perspective on the electron transfer: recovering the Butler–Volmer equation in non-equilibrium thermodynamics. Phys Chem Chem Phys 2016;18:24966–83. https://doi.org/10.1039/C6CP04142F.

[11] Khludnev A, Kovtunenko V. In: Analysis of cracks in solids. Southampton, Boston: WIT-Press; 2000.
[12] Pahon E, Hissel D, Yousfi-Steiner N. A review of accelerated stress tests dedicated to proton exchange membrane fuel cells – part I: fuel cell component level. J Power Sources 2022;546:231895. https://doi.org/10.1016/j.jpowsour.2022.231895.
[13] Ma S, Qin Y, Liu Y, Sun L, Guo Q, Yin Y. Delamination evolution of PEM fuel cell membrane/CL interface under asymmetric RH cycling and CL crack location. Appl Energy 2022;310:118551. https://doi.org/10.1016/j.apenergy.2022.118551.
[14] Qin Y, Ma S, Chang Y, Liu Y, Yin Y, Zhang J, Liu Z, Jiao K, Du Q. Modeling the membrane/CL delamination with the existence of CL crack under RH cycling conditions of PEM fuel cell. Int J Hydrogen Energy 2021;46(12):15850–65. https://doi.org/10.1016/j.ijhydene.2020.12.043.
[15] Takahashi T, Kokubo Y, Murata K, Hotaka O, Hasegawa S, Tachikawa Y, Nishihara M, Matsuda J, Kitahara T, Lyth S, Hayashi A, Sasaki K. Cold start cycling durability of fuel cell stacks for commercial automotive applications. Int J Hydrogen Energy 2022;47(97):41111–23. https://doi.org/10.1016/j.ijhydene.2022.09.172.
[16] Shokhen V, Strandberg L, Skoglundh M, Wickman B. Impact of accelerated stress tests on the cathodic catalytic layer in a proton exchange membrane (PEM) fuel cell studied by identical location scanning electron microscopy. ACS Appl Energy Mater 2022;5(9):11200–12. https://doi.org/10.1021/acsaem.2c01790.
[17] Liu Z, Chen H, Zhang T. Review on system mitigation strategies for start-stop degradation of automotive proton exchange membrane fuel cell. Appl Energy 2022;327:120058. https://doi.org/10.1016/j.apenergy.2022.120058.
[18] Liu Y, Tu Z, Chan S. Catalyst degradation mitigation and fuel utilization enhancement of a dead-ended anode and cathode proton exchange membrane fuel cell with periodical oxygen supply. ACS Sustainable Chem Eng 2022;10(34):11287–98. https://doi.org/10.1021/acssuschemeng.2c03180.
[19] Xu R, Kang L, Papanikolaou K, Wang B, Marlow S, He Q, Zhang P, Wang J, Brett D, Stamatakis M, Wang F. Improving the ORR performance by enhancing the Pt oxidation resistance. J Catal 2022;416:311–21. https://doi.org/10.1016/j.jcat.2022.10.025.
[20] Chu T, Xie M, Yu Y, Wang B, Yang D, Li B, Ming P, Zhang C. Experimental study of the influence of dynamic load cycle and operating parameters on the durability of PEMFC. Energy 2022;239(D):122356. https://doi.org/10.1016/j.energy.2021.122356.
[21] Min J, Kim S, Jeffery A, Shin H, Kang Y, Kim Y, et al. A paradigm shift in CO tolerant catalyst design for fuel cells via introducing defect-controlled carbon molecular sieve layers. Mater Today Energy 2022;29:101124. https://doi.org/10.1016/j.mtener.2022.101124.
[22] Li B, Wan K, Xie M, Chu T, Wang X, Li X, Yang D, Ming P, Zhang C. Durability degradation mechanism and consistency analysis for proton exchange membrane fuel cell stack. Appl Energy 2022;314(8):119020. https://doi.org/10.1016/j.apenergy.2022.119020.
[23] Zuo L, Jian Q, Yang Y. Durability improvement mechanism of proton exchange membrane fuel cell by microporous layer. Int J Energy Res 2022;46(13):18809–18. https://doi.org/10.1002/er.8499.
[24] Goswami N, Grunewald J, Fuller T, Mukherjee P. Mechanistic interactions in polymer electrolyte fuel cell catalyst layer degradation. J Mater Chem 2022;10:15101–15. https://doi.org/10.1039/d2ta02177c.
[25] Choi S-Y, Jin K. Ex situ aging effect on sulfonated poly(ether ether ketone) membrane: hydration-dehydration cycling and hydrothermal treatment. J Energy Chem 2022;70:583–92. https://doi.org/10.1016/j.jechem.2022.03.003.
[26] Heidari H, Esmaili Q, Ranjbar A. Model-based diagnosis of proton-exchange membrane fuel cell cathode catalyst layer microstructure degradation. Int J Energy Res 2022. https://doi.org/10.1002/er.8755.
[27] Huang L, Zhang X, Jiang Y, Huang P, Lin L. Modeling-based analytics of degradation behavior for fuel cell stack under actual dynamic ambient temperature. Energy Convers Manag 2022;269:116100. https://doi.org/10.1016/j.enconman.2022.116100.
[28] Zheng W, Xu L, Hu Z, Zhao Y, Li J, Ouyang M. Dynamic modeling of Pt degradation and mitigation strategies in polymer electrolyte membrane fuel cells. eTransportation 2022;12:100171. https://doi.org/10.1016/j.etran.2022.100171.
[29] Ao Y, Chen K, Laghrouche S, Depernet D. Proton exchange membrane fuel cell degradation model based on catalyst transformation theory. Fuel Cell 2021;21(3):254–68. https://doi.org/10.1002/fuce.202100002.
[30] Kregar A, Gataloc M, Maselj N, Hodnik N, Katrašnik T. Temperature dependent model of carbon supported platinum fuel cell catalyst degradation. J Power Sources 2021;514:230542. https://doi.org/10.1016/j.jpowsour.2021.230542.
[31] Li Y, Moriyama K, Gu W, Arisetty S, Wang C. A one-dimensional Pt degradation model for polymer electrolyte fuel cells. J Electrochem Soc 2015;162(8):F834–42. https://doi.org/10.1149/2.0101508jes.
[32] Liu J, Yin Y, Zhang J, Zhang T, Zhang X, Chen H. Mechanical degradation of catalyst layer under accelerated relative humidity cycling in a polymer electrolyte membrane fuel cell. J Power Sources 2021;512:230487. https://doi.org/10.1016/j.jpowsour.2021.230487.
[33] Du S. Based on one-dimensional nanostructure arrays for proton exchange membrane fuel cell applications. Engineering 2021;7(1):33–49. https://doi.org/10.1016/j.eng.2020.09.014.
[34] Hou J, Yang M, Ke C, Wei G, Zhang J. Optimizing the structural design of a nanocomposite catalyst layer for PEM fuel cells for improving mass-specific power density. Nanoscale 2020;12(26):13858–78. https://doi.org/10.1039/D0NR02421J.
[35] Liu J, Liu S, Yan F, Wen Z, Chen W, Liu X, Liu Q, Shang J, Yu R, Su D, Shui J. Ultrathin nanotube structure for mass-efficient and durable oxygen reduction reaction catalysts in PEM fuel cells. J Am Chem Soc 2022;144(41):19106–14. https://doi.org/10.1021/jacs.2c08361.
[36] Zhang J, Yuan Y, Gao L, Zeng G, Li M, Huang H. Stabilizing Pt-based electrocatalysts for oxygen reduction reaction: fundamental understanding and design strategies. Adv Mater 2021;33(20):2006494. https://doi.org/10.1002/adma.202006494.
[37] Holby E, Morgan D. Application of Pt nanoparticle dissolution and oxidation modeling to understanding degradation in PEM fuel cells. J Electrochem Soc 2012;159(5):B578–91. https://doi.org/10.1149/2.011204jes.
[38] Shimanuki J, Imai H, Ito Y, Nishino Y, Miyazawa A. Microstructural observation of the swollen catalyst layers of fuel cells by cryo-TEM. Microscopy 2022;5(9):11200–12. https://doi.org/10.1093/jmicro/dfac059.
[39] Kovtunenko V, Karpenko-Jereb L. Study of voltage cycling conditions on pt oxidation and dissolution in polymer electrolyte fuel cells. J Power Sources 2021a;493:229693. https://doi.org/10.1016/j.jpowsour.2021.229693.
[40] Kovtunenko V, Karpenko-Jereb L. Lifetime of catalyst under voltage cycling in polymer electrolyte fuel cell due to platinum oxidation and dissolution. Technologies 2021b;9(4):80. https://doi.org/10.3390/technologies9040080.
[41] Pivac I, Barbir F. Impact of shutdown procedures on recovery phenomena of proton exchange membrane fuel cells. Fuel

Cell 2020;160(2):185–95. https://doi.org/10.1002/fuce.201900174.
[42] Kravos A, Ritzberger D, Hametner C, Jakubek S, Katrašnik T. Methodology for efficient parametrisation of electrochemical PEMFC model for virtual observers: model based optimal design of experiments supported by parameter sensitivity analysis. Int J Hydrogen Energy 2021;46(26):13832–44. https://doi.org/10.1016/j.ijhydene.2020.10.146.
[43] Testa E, Maggiore P, Pace L, Vedova MD. Sensitivity analysis for a PEM fuel cell model aimed to optimization. WSEAS Trans Power Syst 2015;10:171–9.
[44] Bi W, Fuller T. Temperature effects on PEM fuel cells Pt/C catalyst degradation. ECS Trans 2007;11(1):1235. https://doi.org/10.1149/1.2781037.
[45] Karpenko-Jereb L, Kelterer A-M, Berezina N, Pimenov A. Conductometric and computational study of cationic polymer membranes in H^+ and Na^+-forms at various hydration levels. J Membr Sci 2013;441:127–38. https://doi.org/10.1016/j.memsci.2013.05.012.
[46] Sethuraman V, Weidner J, Haug A, Motupally S, Protsailo L. Hydrogen peroxide formation rates in a PEMFC anode and cathode: effect of humidity and temperature. J Electrochem Soc 2007;155(1). https://doi.org/10.1149/1.28019800. B50–B57.
[47] Topalov A, Cherevko S, Zeradjanin A, Meier J, Katsounaros I, Mayrhofer KJ. Towards a comprehensive understanding of platinum dissolution in acidic media. Chem Sci 2014;5(2):631–8. https://doi.org/10.1039/c3sc52411f.
[48] Gazdzicki P, Mitzel J, Dreizler AM, Schulze M, Friedrich K. Impact of platinum loading on performance and degradation of polymer electrolyte fuel cell electrodes studied in a rainbow stack. Fuel Cell 2017;18(3):270–8. https://doi.org/10.1002/fuce.201700099.
[49] Shao-Horn Y, Sheng W, Chen S, Ferreira P, Holby E, Morgan D. Instability of supported platinum nanoparticles in low-temperature fuel cells. Top Catal 2007;46:285–305. https://doi.org/10.1007/s11244-007-9000-0.
[50] Cherevko S, Keeley G, Geiger S, Zeradjanin A, Hodnik N, Kulyk N, Mayrhofer K. Dissolution of platinum in the operational range of fuel cells. Chemelectrochem 2015;2(10):1471–8. https://doi.org/10.1002/celc.201500098.
[51] Ahluwalia R, Arisetty S, Wang X, Wang X, Subbaraman R, Ball S, DeCrane S, Myers D. Thermodynamics and kinetics of platinum dissolution from carbon-supported electrocatalysts in aqueous media under potentiostatic and potentiodynamic conditions. J Electrochem Soc 2013;160(4):F447–55. https://doi.org/10.1149/2.018306jes.
[52] Wang X, Kumar R, Myers D. Effect of voltage on platinum dissolution: relevance to polymer electrolyte fuel cells. Electrochem Solid State Lett 2006;9(5):A225–7. https://doi.org/10.1149/1.2180536.
[53] Yu K, Groom D, Wang X, Yang Z, Gummalla M, Ball S, Myers D, Ferreira P. Degradation mechanisms of platinum nanoparticle catalysts in proton exchange membrane fuel cells: the role of particle size. Chem Mater 2014;26(19):5540–8. https://doi.org/10.1021/cm501867c.